Research Article Open Access

Muhammad Ikram\*, Sadia Rehman, Fazle Subhan, Muhammad Nadeem Akhtar, Mutasem Omar Sinnokrot

# Synthesis, characterization, thermal degradation and urease inhibitory studies of the new hydrazide based Schiff base ligand 2-(2-hydroxyphenyl)-3-{[(*E*)-(2-hydroxyphenyl)methylidene]amino}-2,3-dihydroquinazolin-4(1*H*)-one

https://doi.org/10.1515/chem-2017-0035 received August 20, 2017; accepted October 9, 2017.

a

**Abstract:** The novel Schiff base ligand 2-(2-hydroxyphenyl)-3-{[(E)-(2-hydroxyphenyl)methylidene]amino}-2,3dihydroquinazolin-4(1H)-one (H-HHAQ) derived from 2-aminobenzhydrazide was synthesized and characterized by elemental analyses, ES+-MS, 1H and 13C{1H}-NMR, and IR studies. The characterization of the ligand was further confirmed by single crystal analysis. The Schiff base ligand was complexed with metal ions like Co(II), Ni(II), Cu(II) and Zn(II) to obtain the bis-octahedral complexes. The ligand and its metal complexes were also studied for their urease inhibitory activities. All the tested compounds show medium to moderate activities for the enzyme, whereas the copper based complex was found to be much more active against urease with an  $IC_{50} = 0.3 \pm 0.1 \,\mu\text{M}\pm\text{SEM}$ , which is even more potent than the standard thiourea. The IC<sub>ro</sub> of the cobalt complex was 43.4±1.2 µM±SEM, whereas that of the nickel complex was 294.2±5.0 µM±SEM. The ligand H-HHAQ and the zinc complex were inactive against the tested enzyme.

**Keywords:** Schiff base hydrazide ligand, coordination compounds, crystal structure, urease inhibition, kinetic and thermodynamic studies

#### 1 Introduction

Urea amidohydrolases (EC 3.5.1.5), a class of enzymes widespread among all types of organisms ranging from unicellular to higher multicellular organisms, are generally termed as ureases. They are actively involved in the hydrolysis of urea to ammonia and carbamate. The carbamate is divided further to produce another molecule of ammonia. The general reaction catalyzed by urease is shown in scheme 1.

The enzymatic activity can be seen in all forms of organisms like bacteria, fungi, algae and even in man causing elevation in blood pH due to the accumulation of ammonia that leads to the appearance of various effects like cell death, kidney failure, severe ulcer, urolithiasis, pyelonephritis and hepatic encephalopathy, hepatic coma and urinary catheter encrustation [1–14].

Structurally, the enzyme is comprised of two nickel (II) centers each coordinated by two nitrogens from histidines, one water molecule, and a bridging carbamylated lysine through the O atom. The Ni (2) is further coordinated by O-atom from aspartic acid. Therefore, one of the nickels is penta-coordinated whereas the other is hexacoordinated with pseudo square pyramidal geometry for

$$H_2N \xrightarrow{O} + H_2O \xrightarrow{Urease} H_2N \xrightarrow{O} + NH_3 \xrightarrow{H_2O} H_2CO_3 + 2NH_3$$

Scheme 1: Urease catalyzed hydrolysis of urea.

Department of Chemistry, Abdul Wali Khan University, Mardan Pakistan, E-mail: ikram@awkum.edu.pk; sadia@awkum.edu.pk Fazle Subhan: Department of Chemistry, Abdul Wali Khan University, Mardan Pakistan

**Muhammad Nadeem Akhtar:** Department of Chemistry, University of Agriculture, Faisalabad, Pakistan

Mutasem Omar Sinnokrot: Department of Chemistry, The Petroleum Institute, Khalifa University of Science and Technology, Abu Dhabi, 2533 United Arab Emirates

**3** Open Access. © 2017 Muhammad Ikram et al., published by De Gruyter Open. This work is licensed under the Creative Commons Attribution-NonCommercial-NoDerivatives 4.0 License.

<sup>\*</sup>Corresponding author: Muhammad Ikram, Sadia Rehman:

$$\begin{array}{c|c} \text{(Lys)HN} & \text{(Lys)HN} \\ \hline N(\text{His}) & Ni(2) \text{(1)Ni} & Ni(2) \text{(1)Ni} \\ N(\text{His}) & Ni \text{(2)} \text{(1)Ni} & Ni \text{(2)} \text{(1)Ni} \\ N(\text{His}) & Ni \text{(2)} \text{(1)Ni} & Ni \text{(2)} \text{(1)Ni} \\ N(\text{His}) & Ni \text{(2)} \text{(1)Ni} & Ni \text{(2)} \\ N(\text{His}) & Ni \text{(2)} \text{(1)Ni} & Ni \text{(2)} \\ N(\text{His}) & Ni \text{(2)} \\ N(\text{His}) & Ni \text{(2)} \\ N(\text{His}) & Ni \text{(2)} & Ni \text{(2)} \\ N(\text{His}) & N$$

Scheme 2: Mechanism of interaction of inhibitors with urease.

Figure 1: Mechanism of action by different inhibitors (a) by acetohydroxamic acid, (b) by phosphate based molecule, and (c) by boric acid.

the former and pseudo octahedral geometry for the latter respectively. Inhibition of the enzyme is achieved by various methods. One of these include the displacement of the water molecule by the interacting inhibitor as shown in scheme 2.

The mechanism of inhibition of urease for the acetohydroxamic acid, phosphate based compounds and boric acid may be seen in Figure 1.

Urease inhibition by metal complexes has been studied extensively over the last decade [14,15]. The metal complexes bearing the active sites for attachment of -OH group have in particular been found to be very useful in inhibitory studies [14-16]. Recently we studied the Schiff base metal complexes for their inhibitory activities against the human urease enzyme. It has been found that nickel based complexes of 2-[(E)-(quinolin-3-ylimino)methyl]

phenol (H-QMP) [14] were even more potent ( $IC_{50} = 9.9 \pm$ 0.124 µM ± SEM) than the standard thiourea. In another study, we found out that copper based complexes of Schiff baseligands 2-{(E)-[(4-Chlorophenyl)imino]methyl}phenol  $([Cu(CIMP)_2])$  have  $IC_{50} = 10.66 \pm 0.19 \,\mu\text{M} \pm \text{SEM})$  and 2-{(E)-[(4-bromophenyl)imino]methyl}phenol  $([Cu(BIMP)_{3}])$ have  $IC_{50} = 5 \pm 0.047 \,\mu\text{M} \pm \text{SEM}$ , respectively [15]. Changing the environment around the metal center changes the inhibitory activity [16]. The mechanisms of action of metal complexes against urease in these two instances have been explored, and involve either hydrophobic interactions or hydrogen bond formation in the active pocket of the enzyme. Here, in this study we have synthesized a new type of Schiff base ligand bearing both features such as a nitrogen in the cyclic ring and a free hydroxyl group after complexation in order to explore the effect of these groups in the inhibition of the urease enzyme.

# 2 Experimental

#### 2.1 Materials and Methods

All chemicals, and solvents used were of analytical grade. Metal(II) acetates (where metal(II) = Co, Ni, Cu and Zn) were obtained from Riedel-de-Haen, and were partially dehydrated by drying the hydrated salts in a vacuum oven for several hours at 80 - 100°C. 2-aminobenzohydrazine was prepared using the previously reported procedure [17,18]. Salicylaldehyde was obtained from Acros Organics. Solvents were distilled at least twice before use. Unless and otherwise stated, all reactions were carried out under a dinitrogen atmosphere.

#### 2.2 Instrumentation

Elemental analyses were carried out using a Varian Elementar II. Melting points were recorded on a Gallenkamp apparatus. IR spectra were recorded using a Shimadzo FTIR Spectrophotometer Prestige-21. <sup>1</sup>H-NMR were measured with a Bruker DPX 400MHz (400.23 MHz) spectrometer whereas 13C{1H}NMR were recorded on a Bruker AV 400MHz (150.9 MHz) spectrometer, in CDCl<sub>2</sub> at room temperature. Chemical shifts are reported in ppm and standardized by observing signals for residual protons. UV-Visible spectra were recorded on a BMS UV-1602. Molar conductance of the solutions of the metal complexes was determined with a conductivity meter type HI-8333. All measurements were carried out at room temperature with freshly prepared solutions. Magnetic susceptibilities were measured on a Sherwood Gouv Balance at room temperature calibrated with Hg[Co(SCN)]. Mass spectra were recorded on a LCT Orthogonal Acceleration TOF Electrospray mass spectrometer.

#### 2.3 Crystal structure

Single crystal analyses were carried out using an Oxford diffractometer. Suitable single crystals for X-ray structural analyses of H-HHAQ were each mounted on a glass fibre, and the respective data were collected on Oxford diffractometer (graphite-monochromated Mo Kα radiation,  $\lambda = 0.71073$  Å) at 108(2) K. The structure was solved with the olex2.solve [19] structure solution program using Charge Flipping and refined with the olex2.refine [20] refinement package using Gauss-Newton minimisation. Crystallographic details are given in the supplementary information file. CCDC-1036707 (H-HHAQ) data can be obtained free of charge from the Cambridge Crystallographic Data Centre via www.ccdc.cam.ac.uk/ data\_request/cif.

# 2.4 Synthesis of 2-(2-hydroxyphenyl)-3-{[(E)-(2-hydroxyphenyl)methylidenelamino}-2,3dihydroquinazolin-4(1H)-one (H-HHAQ)

Benzohydrazide was prepared by condensing 25 mmol of hydrazine hydrate with 20 mmol of methyl anthranilate in 20 cm<sup>3</sup> of distilled methanol [17,18]. The resulting mixture was stirred and refluxed at 80°C for 3 hrs and the solution was left overnight. Beautiful glassy crystals were isolated after one day, 10 mmol of the benzohydrazide ligand was dissolved in 10 cm3 of distilled methanol and 20 mmol salicyldehyde was added to it. The mixture was stirred for 1hr at room temperature. It was concentrated on a rotary evaporator, after which a yellow Schiff base ligand was obtained, which was washed with copious amounts of 5% n-hexane containing methanol and was recrystallised from THF.

Yield: 76%, D. pt: 223°C, IR: 3500(s), 3387(s), 3155, 3020, 1620(s), 1573(s), 1548, 1514(s), 1450(s), 1367(s), 1325(s), 1280(s), 1257(s), 1172(s), 1132(s), 1060(s), 1035(s), 960(s), 902(s), 866(s), 812(s), 786(s), 740(s), 698(s), 621(s) cm<sup>-1</sup>, <sup>1</sup>H-NMR (400.23 MHz, CD<sub>2</sub>OD, 303k):  $\delta$  = 11.45 (s, 1H, Ar-OH, H27), 9.54 (s, 1H, Ar-OH, H7), 8.27(s, 1H, NH, H19), 7.54 (d,  ${}^{3}J_{HH}$  = 8, aromatic), 7.29 (s, 1H, N-CH-N, H20) 7.19 (t, 2H,  ${}^{3}J_{HH}$  = 7.5, H5 & H24), 7.05(d, 2H,  ${}^{3}J_{HH}$  = 7.5, H6 & H23), 6.83 (d, 4H,  ${}^{3}J_{HH}$  = 7.5, H4, H16, H17 & H25), 6.74 (d, 4H,  ${}^{3}J_{HH}$  = 8.5, H3, H12, H15 & H26), 6.56 (t, 2H,  ${}^{3}J_{HH}$  = 7.5, H4 & H25), 6.35 (s, 1H, CH=N, H8), <sup>13</sup>C{<sup>1</sup>H}-NMR (150.9 MHz, CD<sub>2</sub>OD, 303k),  $\delta$  = 165 (C=0, C11), 160.3 (HC=N-, C8), 153(C, C22), 149.8(CH, C20), 148.7 (CH, C26), 147.9 (CH, C15), 147.5 (C, C1), 133.8 (C, C14), 132 (CH, C23), 128.1 (C, C13), 127.8 (C, C2), 125.9 (CH, C6), 121.9 (CH, C12), 116.2 (CH, C23), 115.3 (CH, C3), 115.4 (C, C21), 113.8 (CH, C5, C4, C24, & C25), 108.7 (CH, C16 & C17), Elemental analyses (C<sub>21</sub>H<sub>17</sub>N<sub>2</sub>O<sub>2</sub>) Calc. C: 70.18%, H: 4.77%, N: 11.69%, EI-MS m/z (%): 382.1168 (88%)  $[C_{21}H_{17}N_3O_3+Na]^+$ ,  $\Lambda_m = 0.10 \mu S$ .

# 2.5 Synthesis of [M(HHAQ),] where M= Co, Ni, Cu and Zn (II) acetates

0.011 mol of metal(II) acetates was stirred in a minimum volume of dried methanol and 0.024 mol of H-HHAQ in a minimum volume of dried methanol was added to the metal solution. The mixture was stirred for 2-3hrs at room temperature. The metal complex was collected after filtration and copiously washed several times with 5% n-hexane containing methanol.

### 2.5.1 Bis(2-(2-hydroxyphenyl)-3-{[(E)-(2-hydroxyphenyl) methylidene]amino}-2,3-dihydroquinazolin-4(1H)-one) cobalt(II) (Co-HHAQ)

Yield: 38%, D. pt: 201 °C, IR: 3240(bd), 3126(bd), 2970(w), 2872(w), 1640(s), 1614(s), 1562(s), 1555(s), 1510(s), 1454(s), 1427(s), 1377(s), 1338(s), 1253(s), 1207(s), 1155(s), 1124(s), 1028(s), 970(s), 893(s), 860(s), 783(s), 750(s), 692(s), 621(s) cm<sup>-1</sup>,  $\lambda_{max}$  = 480, 590, 640 nm ( $\epsilon$  = 67.4, 12.7 M<sup>-1</sup>cm<sup>-1</sup>,  ${}^{4}T_{1}g(F) \rightarrow {}^{4}A_{2}g, {}^{4}T_{1}g(F) \rightarrow {}^{4}T_{1}g(P), {}^{4}T_{1}g(F) \rightarrow {}^{4}T_{2}g), \ \mu_{eff} = 4.98$ B.M. Elemental Analysis ( $C_{42}H_{32}CoN_6O_6$ ), Calc. C: 65.03%, H: 4.16%, N: 10.83%, Co: 7.60%, Exp. C: 66.30%, H: 4.60%, N: 9.59%, Co: 8.12%, EI-MS: m/z (%): 775.1709(67%)  $[C_{42}H_{32}CoN_6O_6]^+$ ,  $\Lambda_m = 10.0 \mu S$ .

## 2.5.2 Bis(2-(2-hydroxyphenyl)-3-{[(E)-(2-hydroxyphenyl) methylidene]amino}-2,3-dihydroquinazolin-4(1H)-one) nickel(II) (Ni-HHAQ)

Yield: 47%, D. pt: 278°C, IR: 3224(bd), 1635(w), 1612(s), 1550(s), 1506(s), 1490(s), 1425(w), 1382(w), 1338(w), 1280(s), 1255(s), 1213(w), 1155(s), 1126(s), 1028(s), 972(s), 931(w), 860(w), 825(w), 792(w), 750(s), 692(s), 615(s), 586(w), 553(w) cm<sup>-1</sup>,  $\lambda_{max}$ = 780(bd) nm [ $\epsilon$  = 12.7 M<sup>-1</sup>cm<sup>-1</sup>,  ${}^{3}A_{2}g(F) \rightarrow {}^{3}T_{1}g(P), {}^{3}A_{2}g(F) \rightarrow {}^{3}T_{1}g(F), {}^{3}A_{2}g(F) \rightarrow {}^{3}T_{2}g(F)], \mu_{eff}$  = 2.88 B.M. Elemental Analysis (C, H, NiO, ), Calc. C: 65.05%, H: 4.16%, N: 10.84%, Ni: 7.57%, Exp. C: 65.12%, H: 4.32%, N: 9.96%, Ni: 7.12%, EI-MS: m/z (%): 774.1731  $[C_{42}H_{22}N_{4}NiO_{4}]^{+}$ ,  $\Lambda_{m} = 4.3 \,\mu\text{S}$ .

### 2.5.3 bis(2-(2-hydroxyphenyl)-3-{[(E)-(2-hydroxyphenyl) methylidenelamino}-2,3-dihydroquinazolin-4(1H)-one) copper(II) (Cu-HHAQ)

Yield: 37%, D. pt: 310°C, IR: 3196(bd), 3066(bd), 2972(bd), 2870(w), 1640(s), 1608(s), 1585(w), 1544(s), 1512(s), 1460(w), 1429(s), 1382(bd), 1278(s), 1201(s), 1155(s), 1124(s), 1053(s), 1028(s), 975(s), 893(s), 856(s), 819(s), 781(s), 750(s), 690(s), 665(s), 615(s), 563(s) cm<sup>-1</sup>,  $\lambda_{max}$  = 820 nm ( $\epsilon$ = 34.7 M<sup>-1</sup>cm<sup>-1</sup>, T<sub>2</sub>g $\rightarrow$ eg),  $\mu_{eff}$  = 1.67 B.M. Elemental Analysis (C<sub>62</sub>H<sub>32</sub>CuN<sub>6</sub>O<sub>6</sub>), Calc. C: 65.65%, H: 4.13%, N: 10.77%, Cu: 7.57%, Exp. C: 65.12%, H: 4.32%, N: 9.96%, Ni: 7.12%, EI-MS: m/z (%): 779.167934 [C<sub>42</sub>H<sub>32</sub>CuN<sub>6</sub>O<sub>6</sub>]<sup>+</sup>,  $\Lambda_m = 87 \mu S$ .

#### 2.5.4 bis(2-(2-hydroxyphenyl)-3-{[(E)-(2-hydroxyphenyl) methylidene]amino}-2,3-dihydroquinazolin-4(1H)-one) zinc(II) (Zn-HHAQ)

Yield: 32%, D. pt: 210°C, IR: 3251(bd), 2968(w), 2870(w), 2366(w), 1687(w), 1614(s), 1585(s), 1564(s), 1510(s), 1427(s), 1384(s), 1334(w), 1278(w), 1253(s), 1205(s), 1155(s), 1124(s), 1028(s), 970(s), 896(s), 858(s), 821(s), 783(s), 748(s), 692(s), 665(s), 615(s), 582(s), 543(s) cm<sup>-1</sup>, Elemental Analysis (C<sub>42</sub>H<sub>22</sub>N<sub>2</sub>O<sub>2</sub>Zn), Calc. C: 64.50%, H: 4.12%, N: 10.74%, Zn: 8.36%, Exp. C: 64.67%, H: 4.82%, N: 10.44%, Zn: 8.12%, EI-MS: m/z (%): 780.1669(23)  $[C_{42}H_{22}N_{4}O_{4}Zn]^{+}$ ,  $\Lambda_{m} = 54 \mu S$ .

#### 2.6 Urease inhibition assay

Exactly 25 µL of enzyme (jack bean urease) solution and 5 µL of test compound (0.5 mM concentration) were incubated with 55 µL of buffer containing 100 mM urea for 15 min at 30 °C in each well of a 96-well plate. Ammonia production was measured as a measure of urease activity by the indophenol method. Final volumes were maintained as 200 µL by adding 45 µL of a phenol reagent (1% w/v phenol and 0.005% w/v sodium nitroprussside), and 70 μL of an alkali reagent (0.5% w/v NaOH and 0.1% active chloride NaOCl) to each well. Using a microplate reader (Molecular Devices, CA, USA), the increase in absorbance was measured at 630 nm after 50 min at pH 6.8 [21,22].

## 2.7 TG-DTA analysis

The TG-DTA analyses were carried out using TG/DTA Diamond model by Perkin Elmer at a heating rate of 10°C min<sup>-1</sup> in a temperature range of 30-1000°C under static air. The specific mass of samples were contained in ceramic pan crucibles adjusted on a platform support giving a proportional signal to recorder, observed by a computer interface and the results were plotted in the form of mass loss of sample vs. temperature for TG and microvolts vs. temperature for DTA. All the results were referenced to the thermal decomposition of alumina. The activation energies of all of the samples were calculated using the Horowitz-Metzger method [23]. It was found that linear plots could be obtained while  $\ln (Wo - W_1^f)/(W - W_1^f)$  {where Wo = initialmass taken, W = weight remaining at a given temperature,  $W_{\star}^{f}$  = final weight} were plotted against  $\Theta$  {where  $\Theta = T_{c}$ -T<sub>a</sub>}. The slope of the straight line was used to calculate the activation energy through the expression (1):

Slope = 
$$E^*/RT_c^2$$
 (1)

The order of decomposition was calculated from the relationship between the reaction order and concentration at maximum slope [23]. Thermodynamic parameters of activation were evaluated by using the following expressions (2), (3) and (4), respectively [24]:

$$\Delta S^* = 2.303 \log[Ah/k_B T_s]R \tag{2}$$

$$\Delta H^* = \Delta E^* - RT \tag{3}$$

$$\Delta G^* = \Delta H^* - T \Delta S^* \tag{4}$$

Ethical approval: The conducted research is not related to either human or animals use.

# 3 Results and discussion of H-HHAQ series

## 3.1 Analytical and spectroscopic characterization

The novel Schiff base ligand 2-(2-hydroxyphenyl)-3-{[(E)-(2-hydroxyphenyl)methylidene]amino}-2,3dihydroquinazolin-4(1H)-one (H-HHAQ) and its first row divalent metal complexes were characterized using different spectroscopic and analytical methods. By looking at the structure of the ligand, it becomes apparent that the

aromatic protons are in the same environment, therefore the <sup>1</sup>H-NMR spectrum of the ligand show four doublets and two triplets in the region 6.5-7.6 ppm. Five singlets were also observed along with these aromatic bands. Singlets at 11.45 ppm and 6.34 ppm were assigned to the two hydroxyl groups. The difference in the values was assigned to the probable involvement of one of the hydroxyl groups in hydrogen bonding with the nitrogen of the Schiff base linkage. The other hydroxyl group is considered to be freely available as may also be seen in the crystal structure. The HC=N proton appears at 9.45 ppm as expected. A singlet at 8.25 ppm was assigned to the cyclic NH group. A singlet at 7.29 ppm was assigned to the cyclic N-CH-N proton. The <sup>13</sup>C{<sup>1</sup>H}-NMR recorded also show similar peaks for the secondary and tertiary carbon atoms. The ketonic carbon was observed at 165 ppm, whereas the -CH=N was observed at around 160 ppm. C1 and C22 were observed at 147 and 153 ppm respectively which were assigned to the carbon atoms with the hydroxyl groups. The rest of the 13C-NMR spectrum was assigned unambiguously to the respective secondary and tertiary carbon atoms.

The ligand H-HHAQ was reacted with divalent metal ions like Co(II), Ni(II), Cu(II) and Zn(II) and bis-complexes were obtained as may be seen in scheme 3.

All the complexes were characterized by elemental analyses, ES+-MS, UV-visible and IR spectroscopic techniques. The elemental analyses supported by the ES<sup>+</sup>-MS results confirmed the mentioned compositions.

The IR spectra were also recorded in the region 4000-600 cm<sup>-1</sup>, which show that the complex formation occurs through coordination from Schiff base linkage, hydroxyl group and the cyclic ketone group. In the free ligand and the complexes these linked groups were found to be varying in the range of  $\Delta v = 40-60 \text{ cm}^{-1}$ . In the free ligand the −OH group was observed in the region 3500 cm<sup>-1</sup> which is further broadened and moved to 3200 cm<sup>-1</sup> after formation of the complexes. The cyclic ketone group was observed around 1620 cm<sup>-1</sup> which was moved to 1640 cm<sup>-1</sup> in Co-HHAQ, Ni-HHAQ and Cu-HHAQ whereas in Zn-HHAQ it is moved to 1680 cm<sup>-1</sup>. Similarly the Schiff base linkage was observed around 1573 cm<sup>-1</sup> as a strong peak which was found around 1620 cm<sup>-1</sup> in all of the complexes. Therefore it was confirmed that these functional groups are involved in the formation of the octahedral metal complexes.

The UV-Visible spectra of Co-HHAQ, Ni-HHAQ and Cu-HHAQ were recorded in the range 200-800 nm in a 1 cm matched quartz cuvette. The compound Co-HHAQ was found to absorb visible light and gave three peaks at 480, 590 and 640 nm. These peaks were assigned to the  ${}^{4}\text{T}_{1}\text{g}$  (F)  $\rightarrow {}^{4}\text{A}_{2}\text{g}$  and the  ${}^{4}\text{T}_{1}\text{g}$  (F)  $\rightarrow {}^{4}\text{T}_{1}\text{g}$  (P),  ${}^{4}\text{T}_{1}\text{g}$  (F)  $\rightarrow {}^{4}\text{T}_{2}\text{g}$ transitions, respectively [25,26]. It means that carbonyl

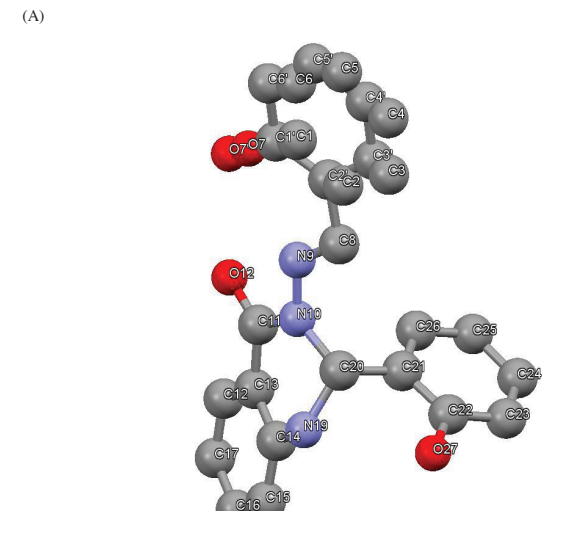
Scheme 3: Formation of Octahedral complexes of HHAQ with M(II) ions where M = Co, Ni, Cu and Zn.

group, hydroxyl ion and the Schiff base linkage are involved in the formation of octahedral geometry. The ligand is responsible for the high spin electronic configuration of the complex as suggested by the magnetic susceptibility value. The compound Ni-HHAQ was found to be absorbing in the range of 780 nm as a broad peak which might be encompassing the overlapping peaks. Therefore this broad spectral line may be assigned to the possible transition caused by  ${}^{3}A_{3}g$  (F)  $\rightarrow {}^{3}T_{1}g$  (P),  ${}^{3}A_{3}g$  (F)  $\rightarrow {}^{3}T_{1}g$  (F), and  ${}^{3}A_{2}g(F) \rightarrow {}^{3}T_{2}g(F)$ . The magnetic susceptibility value of the compound shows that the complex is high spin having two unpaired electrons in the eg level. Similarly the copper complex Cu-HHAQ of this ligand is absorbing in the form of broad peak in the range of 820 nm. This transition may be due to  $T_2g \rightarrow eg$  [25,26]. The complex has  $\mu_{eff} = 1.67$  B.M. representing the paramagnetic nature with one unpaired electron in the eg level. The complex **Zn-HHAQ** was found to be diamagnetic in nature, therefore did not correspond to any magnetic effects.

Compounds Co-HHAQ and Ni-HHAQ were found to be non-electrolytic in nature as depicted from their molar conductance values, whereas compounds Cu-HHAQ and Zn-HHAQ show small values for the conductance which may be due to the free availability of the proton on the non-coordinating hydroxyl group.

#### 3.2 Crystal Structure of H-HHAQ

**H-HHAQ** was crystallised from THF with a C222, space group after keeping the solution for 12hrs at room temperature, after which a yellow block single crystal was isolated. The ORTEP plot (Figure 2) of H-HHAQ show a Schiff base linkage at C(8) and N(9). C(20), a chiral carbon, may be seen in the formation of distorted heterocyclic ring system connecting both N(19) and N(10). Due to this unique linkage the three aromatic rings lie at angle less than 180°, creating a three dimensional orientation. The plane produced by the aromatic ring C(8)-C(1)-C(3)-C(4)-C(5)-C(6) is therefore lying at 32.45° to the plane produced



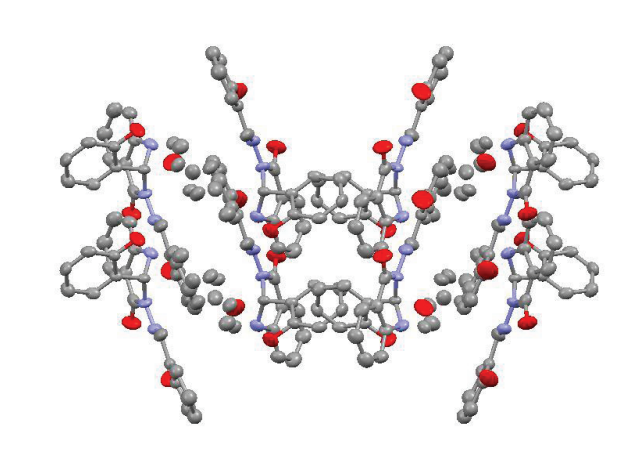


Figure 2: (A) Molecular structure of H-HHAQ. Thermal ellipsoids are shown at 50% probability, and (B) Crystal packing diagram of H-HHAQ. H atoms are omitted for reasons of clarity for both (A) and (B).

by C(12)-C(13)-C(14)-C(15)-C(16)-C(17) aromatic ring. C(20) was found to be 32.49° below the plane produced by C(12)-C(13)-C(15)-C(16)-C(17) aromatic ring.

Therefore it can be concluded that C(20) is involved in the distortion of both aromatic rings. Similarly the plane produced by N(10)-C(11)-C(13)-C(14)-N(19) is also 32.49° above than C(20). The distance between C(8)-N(9) is 1.292 Å, which is equal to the normal bond length of imine linkage as found in (E)-4-bromo-2-[(2-chloro-3-pyridyl)-iminomethyl] phenol (1.291 Å) [27]. The C(20)-N(10) and C(20)-N(19) bond lengths are 1.458 Å and 1.452 Å respectively with a 0.006 Å difference. These bond lengths may be compared with 1.437 Å in 2,2',2",2"'-(1,4-Phenylenedinitrilo)tetraacetic acid dehydrate [28]. The ligand H-HHAQ crystalizes in splits for phenyl groups reasonably to greater extent that the electron density for the carbon atoms can be justified only in sense that reflection of the two groups are considered.

Table 1: Crystal data and structure refinement for H-HHAQ.

Identification code	H-HHAQ
Empirical formula	$C_{21}H_{17}N_3O_3$
Formula weight	359.38
Temperature/K	295(2)
Crystal system	orthorhombic
Space group	C222 <sub>1</sub>
a/Å	10.2571(9)
b/Å	14.4341(12)
c/Å	23.706(2)
α/°	90
β/°	90
γ/°	90
Volume/ų	3509.7(5)
Z	8
$\rho_{calc}g/cm^3$	1.360
μ/mm <sup>-1</sup>	0.093
F(000)	1504.0
Radiation	MoKα ( $λ = 0.71073$ )
2Θ range for data	5.9 to 53.912
collection/°	
Index ranges	-12 ≤ h ≤ 6, -17 ≤ k ≤ 16, -28 ≤ l ≤ 29
Reflections collected	5355
Independent reflections	3037 [ $R_{int} = 0.0718$ , $R_{sigma} = 0.1716$ ]
Data/restraints/parameters	3037/55/255
Goodness-of-fit on F <sup>2</sup>	0.998
Final R indexes [I>= $2\sigma$ (I)]	$R_1 = 0.0820$ , $wR_2 = 0.0650$
Final R indexes [all data]	$R_1 = 0.1888$ , $wR_2 = 0.0886$
Largest diff. peak/hole /	0.18/-0.23
e Å <sup>-3</sup>	
Flack parameter	0.5(10)

Table 2: Selected bond lengths of H-HHAQ.

Moiety	Bond length (Å)	Moiety	Bond length (Å)
		Molety	Dona tength (A)
C1'-07'	1.359(18)	N10-C20	1.463(8)
C1-07	1.374(12)	C11-O12	1.240(9)
C2-C8	1.471(11)	C20-C21	1.512(7)
C2'-C8	1.447(15)	C14-N19	1.385(9)
C8-N9	1.275(9)	N19-C20	1.457(9)
N9-N10	1.362(8)	C22-O27	1.368(7)
N10-C11	1.382(8)	C20-C21	1.512(7)

This crystal structure is completely different from the one reported earlier [29]. The electron density of phenolic ring is duplicated upon refinement. The molecule bears intra and intermolecular hydrogen bonding. The intramolecular H-bond is found between two sets of atoms like O27... H19 = 2.466 Å and N9...H7 = 1.989 Å. The intermolecular H-bond is found between O12 and H27 of 1.939 Å length. The molecular packing diagram is shown in Figure 2B revealing the butterfly structure of the ligand. The crystal data, selected bond lengths and bond angles are shown in tables 1, 2 and 3 respectively.

Table 3: Selected bond angles of H-HHAQ.

Moiety	Bond angle (º)	Moiety	Bond angle (º)
07'-C1'-C2'	126(3)	012-C11-C13	125.1(8)
07'-C1'-C6'	114(3)	N10-C11-C13	115.5(7)
C2'-C1'-C6'	120.0	C15-C14-N19	122.3(8)
07-C1-C2	123.1(16)	C13-C14-N19	117.7(8)
07-C1-C6	116.8(16)	C14-N19-C20	115.7(7)
C2-1-C6	120.0	N19-C20-N10	107.5(6)
C1-C2-C3	120.0	N19-C20-C21	113.6(6)
C3-C2-C8	124.1(9)	N10-C20-C21	113.3(6)
N9-C8-C2	128.6(10)	C26-C21-C22	118.1(6)
C8-N9-N10	121.9(7)	C26-C21-C20	124.1(7)
N9-N10-C11	115.7(7)	C22-C21-C20	117.8(7)
N9-N10-C20	123.5(6)	027-C22-C23	122.9(7)
C11-N10-C20	120.5(7)	027-C22-C21	116.4(6)
012-C11-N10	119.4(8)		

#### 3.3 Enzyme inhibitory activities

Urease (urea amidohydrolase EC 3.5.15) is a nickel containing metalloenzyme which catalyzes the hydrolysis of urea to ammonia and carbon dioxide as may be seen in scheme 1. Urease is involved in the function to use urea as nitrogen source [1-16] and is known to be the major cause of diseases induced by H. pylori, thus allow them to survive at low pH inside the stomach and thereby play an important role in the pathogenesis of gastric and peptic ulcer, apart from cancer as well [1-16]. Urease is directly involved in the formation of infection stones and contributes to the pathogenesis of urolithiasis, pyelonephritis, and hepatic encephalopathy, hepatic coma and urinary catheter encrustation. Previously reported bismuth complexes are one of the widely used compounds for the treatment of peptic ulcers and Helicobacter pylori infections as urease inhibitors [1-16]. Bismuth complexes exhibited many side effects such as darkening of tongue, vomiting, diarrhea, dizziness. To overcome these side effects we have synthesized various metal complexes of Schiff-base ligands [14-16] and were tested for their potential inhibition against the urease enzyme. Here we extended our quest for successful and selective urease inhibitor development.

The H-HHAQ and its complexes were studied for their inhibitory activities against the urease enzyme in optimum conditions and the results are shown in table 4. Table 4 shows that the copper complex **Cu-HHAQ**, is acting as an inhibitor for the inhibition of urease activity. Other complexes like **Co-HHAQ** and **Ni-HHAQ**, are active for inhibiting the activity of urease whereas Zn-HHAQ is not active for the enzyme. Therefore, Cu-HHAQ may act as drug for the treatment of diseases related to urease and butyrylcholinesterase adding to the metal based drugs.

It was found that all the metal containing derivatives of **HHAQ** are active except the zinc based derivative. The nickel containing compound Ni-HHAQ is also moderately active. Previously, the Schiff base containing metal complex Bis(2-[(E)-(quinolin-3-vlimino)methyl] phenolato)nickel(II) has been reported with the inhibitory activity  $IC_{50} = 9.9 \pm 0.124 \mu M \pm SEM$ . Here in this work, the compound **Ni-HHAQ** showed IC<sub>50</sub> = 294.2  $\pm 5.0 \mu M \pm SEM$ which is higher in comparison to the above example. The activities of the metal complexes against urease enzyme show that copper based metal complex of HHAQ are more active than the other counterparts. The activity may be compared with reported examples like Bis(2-{(E)-[(4-chlorophenyl)imino]methyl}phenolate)copper(II) with  $IC_{50} \pm S.E.M. = 10.7 \pm 0.2 \,\mu\text{M}$  whereas Bis(2-{(E)-[(4bromophenyl)imino]methyl}phenolate)copper(II) shown  $IC_{50}$  ±S.E.M. = 5.0±0.1  $\mu$ M [14, 15]. The activities of these copper complexes are far less than the activity shown by the copper complex with **H-HHAQ** ligand. The inhibitory activity of the compound Cu-HHAQ may be explained by geometric constraints created by the ligand around the central metal ion. The ligand in its coordinated form also offers coordinating sites for possible interaction with the Ni center of urease enzyme. There may be an interaction with the OH bridge group in the enzyme which may lead to enzymatic activities. One or more than one effect may be involved in enzyme inhibition therefore; some complexes have shown moderate whereas others have shown strong

Table 4: Urease Inhibition by metal complexes of H-HHAQ.

Compound	Conc. (mM)	% Inhibition	IC <sub>50</sub> (μM±SEM)
H-HHAQ	0.5	18.6	
1	0.5	88.9	43.4±1.2
2	0.5	94.0	294.2±5.0
3	0.5	99.9	0.3±0.1
4	0.5	38.5	
Thiourea	0.5	96.9	21.8±1.26

inhibition. The active compounds may further be studied in vivo for possible urease metal based drug.

### 3.4 Thermodynamics and Thermal studies

Thermal degradation of the ligand H-HHAQ and its divalent metal complexes were evaluated in the temperature range 30-1000°C. The thermal pyrolysis in the form of TG curves, is shown in Figure 3 and the corresponding DTA peaks are shown in Figure 4. Based upon the Td temperatures the order of stability may vary viz; 220°C, 225°C, 230°C and 550°C for Co-HHAQ, Ni-HHAQ, Cu-HHAQ and Zn-HHAQ respectively. For ligand H-HHAQ the Td temperature is 245°C. TG and DTA curves are shown in Figure 3 and 4 respectively for **H-HHAQ** and its metal complexes, whereas the data obtained from TG and DTA are shown in table 5 and 6 respectively.

By comparing the data in Table 6, it is clear that the ligand and all its metal complexes decompose in a two step degradation process. The difference between the ligand and the metal complexes lie in the final step, for the ligand no residue is found whereas the decomposition of complexes left behind metal or the corresponding oxides as residues. From Table 5 it is apparent that the ligand has 8.75 KJ/mol activation energy and follow 5th order kinetics for its decomposition. The negative entropy value and a high Gibbs free energy term represent that decomposition is not favored for the parent compound.

H-HHAQ follows the two step degradation, including the formation of free radicals like phenol and benzene. The two phenol free radicals combine together to produce the fused biphenylenediol. Along with bipheneylenediol one mole of carbon monoxide gas and one mole of nitrogen gas are released in the first step. In the second step the benzene free radical produces the cyclohexa-1,3diene-5-vne as a product along with one mole of acetylene [14], half a mole of dinitrogen and dihydrogen gases. The degradation route is shown below in scheme 4.

Table 5: Kinetic and thermodynamic parameters of H-HHAQ and its metal complexes.

Compound	Ts in K	Ea, KJ/mol	ΔH, KJ/mol	ΔG#, KJ/mol	ΔS#, Jmol <sup>-1</sup> K <sup>-1</sup>	Order of reaction, n
H-HHAQ	526.5	8.75	4.37	136.30	-250.56	5
1	501.6	20.30	16.1	138	-243.03	∞
2	775.5	12.00	5.5	202	-253.33	2
3	560	20.8	16.2	154.76	-247.5	5
4	855.7	31.65	24.53	248.74	-262.02	1/2

Table 6: Thermo analytical results of H-HHAQ and its complexes.

Compound	TG Temp. range/	Stage	Mass loss		DTA	Moiety evolved
	°C , G ,		% Calc.	% Found		•
H-HHAQ	30-400	T	67.3	66.2	(+)5, (-)18,	N <sub>2</sub> , CO, C <sub>12</sub> H <sub>10</sub> O <sub>2</sub>
	400-600	II	32.3	33.8	(-)22, (-)25	C <sub>6</sub> H <sub>4</sub> , C <sub>2</sub> H <sub>2</sub> , 1/2N <sub>2</sub> , 1/2H <sub>2</sub>
1	30-280	1	18.8	17.0	(-)2, (+)8	$C_{12}H_{8}$
	280-620	II	69.6	68.1	(+)32, (-)15	$2 C_{12} H_{10} O_2$ , 2CO, $C_2 H_2$ , $3/2 N_2$ , $H_2$
	>620	Res	9.6	11.3		CoO
2	30-390	1	39.9	39.2	(-)12, (-)9, (-)18	C <sub>12</sub> H <sub>8</sub> , 3N2, C <sub>2</sub> H <sub>2</sub> , 2CO
	390-640	II	47.9	47.2	(-)38, (+)1, (-)14, (-)29	$2 C_{12} H_{10} O_2$
	>640	Res	10.5	11.4		NiO
3	30-450	I	55.6	56.0	(-)5.8, (-)5.6, (-)15.3, (-)18	$C_{12}H_{8,} 1/2N_{2}, 2CO, 2C_{2}H_{2,}$ $N_{2}O_{4}$
	450-600	II	48.2	48.2	(-)12.0	2 C <sub>12</sub> H <sub>10</sub> O <sub>2</sub>
	>600	Res	10.1	10.9		CuO
4	30-380	1	47.9	47.5	(-)0.5, (+)5.6, (-)5.3	$C_{12}H_{8,}3N_{2}$ , 2CO, $2C_{2}H_{2}$
	380-680	II	48.8	49.9	(-)5.0	$2 C_{12} H_{10} O_2$
	>680	Res	6.8	5.1		Zn

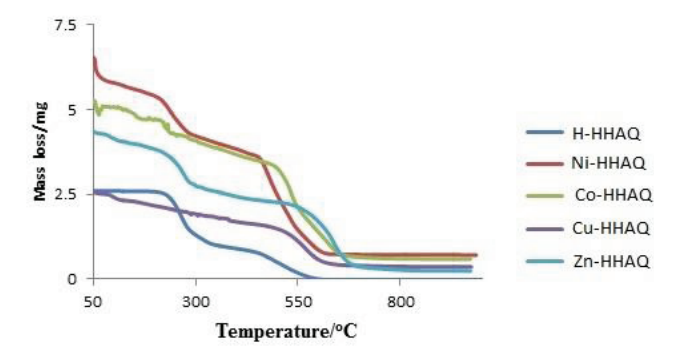
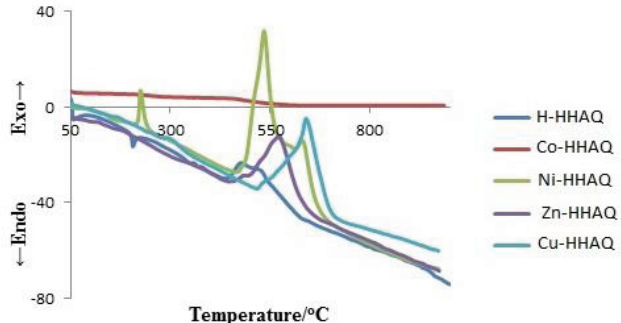


Figure 3: Thermogravimetric plots of H-HHAQ and its metal complexes.

**Co-HHAQ** follows thermal degradation in two steps, in the first step the two free radicals of benzene are produced which combine together to produce bipheylene. There are two exothermic DTA peaks for the first step of pyrolysis. In the second stage two moles of acetylene, 3/2 moles of nitrogen, and two moles of biphenylenediol are produced [15]. Cobalt oxide remains as a residue. There are two exothermic DTA peaks observed for the second step of pyrolysis. It has a negative entropy of activation, and a high value of Gibbs free energy of activation and a reasonable enthalpy of activation. According to the Horowitz method, compound **Co-HHAQ** follows an infinite order of degradation. The degradation route is shown in scheme 5.



**Figure 4:** Differential thermogravimetric curves for H-HHAQ and its metal complexes.

$$C_{21}H_{17}N_3O_3 \Rightarrow C_{12}H_{10}O_2 + CO + N_2 + C_8H_7N$$
 I Stage 
$$C_8H_7N \Rightarrow C_6H_4 + C_2H_2 + 1/2H_2 + 1/2N_2$$
 II Stage

Scheme 4: Thermal degradation of H-HHAQ.

The decomposition of the **Ni-HHAQ** starts at 220°C and ends at 650°C producing nickel oxide as a residue. It also follows a two step degradation; the first step is the same as for complound **Co-HHAQ**, with the production of biphenylene. This step of degradation is represented by the production of two intermediate free radicals of benzene moiety. Apart from this, two moles of carbon monoxide and acetylene and three moles of dinitrogen, are also produced. Three DTA peaks are observed for this stage, including one exothermic and two endothermic

peaks. The fusion of two benzene free radicals to produce biphenylene is an endothermic process. The second stage of degradation is represented by the production of the same phenol free radicals which may combine together producing two moles of biphenol as whole in the degradation process. Nickel oxide remains as a residue in the whole degradation process of Ni-HHAQ. The second stage is represented by a marked exothermic DTA peak having the other two as shoulder counterparts. The activation energy of Ni-HHAQ is lower than Co-HHAQ and follows second order degradative kinetics. The entropy value is more negative than Co-HHAQ and also the Gibbs free energy of activation is also high depicting the stable nature of the parent compounds. The degradative route is shown in scheme 6.

For compound Cu-HHAQ the oxidative degradation starts at 450°C with the release of the same biphenylene product after the reaction between the two benzene free radicals with each other [14,15]. It is accompanied by the release of two moles each of the acetylene and carbon monoxide gases. Apart from this, one mole each of nitrogen dioxide and dinitrogen tetra oxide are also released, the latter of which may undergo further decomposition adding to the molar quantity of nitrogen dioxide. This stage of pyrolysis depicts four exothermic DTA peaks. The second and final stage of pyrolysis is accompanied by the release of a biphenol moiety leaving behind the copper oxide as the residue. This step has one huge exothermic DTA peak. If Table 5 is consulted for the thermodynamic parameters it can be seen that the entropy of activation for Cu-HHAQ is more negative than Co-HHAQ and more positive than Ni-HHAQ. The same trend can be seen for the Gibbs free energy of activation; while the enthalpy change of activation is almost equal to Co-HHAQ. The activation energy is higher than both Co-HHAQ and Ni-**HHAQ** and follows 5<sup>th</sup> order kinetics. The decomposition of the compound may be seen in scheme 7.

The decomposition for **Zn-HHAQ** starts at around 230°C and completes at 680°C. The whole degradation of the compound takes place in two steps. In the first step biphenylene is produced by the fusion of benzene free radicals along with the release of three moles of dinitrogen, two moles of acetylene and two moles of carbon monoxide. The whole degradation is comprised of four DTA peaks, all of them are exothermic. This includes three exothermic DTA peaks for the first stage of decomposition and one huge DTA peak for the second stage of decomposition. The second stage of decomposition releases the biphenol moiety, whereas zinc remains as a residue in the metallic state. The degradation is shown in the scheme 8.

$$C_{42}H_{32}N_6O_6Co \rightarrow C_{12}H_8 + C_{30}H_{24}CoN_6O_6$$
 | I Stage

$$C_{30}H_{24}CoN_6O_6 + O_2 \rightarrow 2C_{12}H_{10}O_2 + 2C_2H_2 + 3/2N_2 + CoO$$
 II Stage

Scheme 5: Thermal degradation of Co-HHAQ.

$$C_{24}H_{20}NiO_4 + O_2 \rightarrow 2C_{12}H_{10}O_2 + NiO$$
 II Stage

Scheme 6: Thermal degradation of Ni-HHAQ.

$$\begin{aligned} &C_{_{42}}H_{_{32}}CuN_{_{6}}O_{_{6}} \Rightarrow C_{_{12}}H_{_{8}} + 1/2N_{_{2}} + 2CO + 2C_{_{2}}H_{_{2}} + \\ &+ NO_{_{2}} + 2N_{_{2}}O_{_{4}} + C_{_{24}}H_{_{20}}CuO_{_{4}} \end{aligned} \qquad \text{I Stage}$$

$$C_{34}H_{30}CuO_4 + O_2 \rightarrow 2C_{12}H_{10}O_2 + CuO$$
 II Stage

Scheme 7: Thermal degradation of Cu-HHAQ.

$$C_{42}H_{32}N_6O_6Zn \rightarrow C_{12}H_8 + 3N_2 + 2CO + 2C_2H_2 + C_{24}H_{20}O_4Zn$$
 I Stage

$$C_{24}H_{20}O_4Zn \rightarrow 2C_{12}H_{10}O_2 + Zn$$
 II Stage

Scheme 8: Thermal degradation of Zn-HHAQ.

By comparing the data in table 5 it becomes clear that the values of activation energy, change in entropy of activation, change in Gibbs free energy of activation, change in enthalpy of activation are higher for **Zn-HHAQ** than any other complex of the same ligand. Therefore zinc produces the stable complex with H-HHAQ, representing that the degradation is less favored in this case.

# **4 Conclusion**

The novel Schiff base ligand **H-HHAQ** was synthesized from aminobenzohydrazin which is actually a heterocyclic derivative of salicyldehyde. It was complexed with divalent metal ions like Co(II), Ni(II), Cu(II) and Zn(II) to yield octahedral metal complexes. The ligand and its metal complexes were completely characterized by different analytical and spectroscopic techniques and was assigned composition and structures. Apart from this, the ligand was also characterized by single crystal studies and it was determined that intermolecular and intramolecular hydrogen bonding is responsible for the crystal packing of the ligand. All the compounds were studied for their inhibiting activities against urease enzyme. It was observed that copper based metal complex of **H-HHAQ** ligand was active with an IC<sub>50</sub> = 0.3  $\pm$  0.1  $\mu$ M $\pm$ SEM which is

even more potent than the standard thiourea. The cobalt complex showed an  $IC_{50}$  of 43.4±1.2  $\mu$ M±SEM, whereas for the nickel complex, this was 294.2±5.0 µM±SEM. Therefore it becomes apparent that the Cu-HHAQ based drug for the diseases related to urease enzyme can be designed. The thermal degradation of the compounds revealed that the order of decreasing activation energies was  $E^*_{7n} < E^*_{7n}$ <E\*, and the order of decreasing stability was Zn(II) <Cu(II) < Co(II) < Ni(II).

**Conflict of interest:** Authors state no conflict of interest.

## References

- [1] Zaborska W., Krajewska B., Leszko M., Olech Z., Inhibition of urease by Ni<sup>2+</sup> ions. Analysis of reaction progress curves, J. Mol. Catal. B Enzym., 2001, 13, 103-108.
- Karplus P.A., Pearson M.A., Hausinger R.P., 70 years of crystalline urease: what have we learned? Acc. Chem. Res. 1997, 30, 330-337.
- [3] Zaborska W., Kot M., Superata K., Evaluation of the inhibition mechanism, J. Enzym. Inhib. Med. Chem., 2002, 17, 247-253.
- [4] Li H.-Q., Xiao Z.-P., Luo Y.-L., Yan T., Lv P.-C., Zhu H.-L., Amines and oximes derived from deoxybenzoins as Helicobacter pylori urease inhibitors, Eur. J. Med. Chem., 2009, 44, 2246-2251.
- Mao W.-J., Lv P.-C., Shi L., Li H.-Q., Zhu H.-L., Synthesis, molecular docking and biological evaluation of metronidazole derivatives as potent Helicobacter pylori urease inhibitors, Bioorg. Med. Chem., 2009, 17, 7531-7536.
- Xiao Z.-P., Shi D.-H., Li H.-Q., Zhang L.-N., Xu C., Zhu H.-L., Polyphenols based on isoflavones as inhibitors of Helicobacter pylori Urease, Bioorg. Med. Chem., 2007, 15, 3703-3710
- [7] Zaborska W., Krajewska B., Olech Z., Heavy metal ions inhibition of jack bean urease: potential for rapid contaminant probing, J. Enzym. Inhib. Med. Chem., 2004, 19, 65-69.
- [8] Amtul Z., Atta-ur-Rahman, Siddiqui R.A., Choudhary M.I., Chemistry and Mechanism of Urease Inhibition, Curr, Med. Chem., 2002, 9, 1323-1348,
- Ara R., Ashiq U., Mahroof-Tahir M., Maqsood Z.T., Khan K.M., Lodhi M.A. Choudhary M.I., Chemistry, urease inhibition, and phytotoxic studies of binuclear vanadium(IV) complexes, Chem. Biodivers., 2007, 4, 58-71.
- [10] Hou P., You Z.-L., Zhang L., Ma X.-L., Ni L.-L., Synthesis, characterization, and DNA-binding properties of copper(II), cobalt(II), and nickel(II) complexes with salicylaldehyde 2-phenylquinoline-4-carboylhydrazone, Trans. Met. Chem., 2008, 33, 267-273.
- [11] Cheng K., Zheng Q.-Z,. Zhu H.-L., Syntheses, structures and urease inhibitory activities of mononuclear cobalt(III) and 1D cobalt(II) complexes with ligands derived from 3-formylsalicylic acid, Inorg. Chem. Commun., 2009, 12, 1116-1119.
- [12] Cheng K., You Z.-L., Zhu H.-L., New method for the synthesis of a mononucleating cyclic peptide ligand, crystal structures of its Ni, Zn, Cu, and Co complexes, and their Inhibitory bioactivity against urease, Aust. J. Chem., 2007, 60, 375-379.

- [13] You Z.-L., Ni L.-L., Shi D.-H., Bai S., Synthesis, structures, and urease inhibitory activities of three copper(II) and zinc(II) complexes with 2-{[2-(2-hydroxyethylamino)ethylimino] methyl}-4-nitrophenol, Eur. J. Med. Chem., 2010, 45, 3196-
- [14] Ikram M., Rehman S., Faridoon, Baker R.J., Rehman H.U., Khan A., Choudhary M.I., Rehman S.-U., Synthesis and distinct urease enzyme inhibitory activities of metal complexes of Schiff-base ligands: Kinetic and thermodynamic parameters evaluation from TG-DTA analysis, Thermochim. Acta, 2013, 555,
- [15] Ikram M., Rehman S., Ali M., Faridoon, Schulzke C., Baker R.J., Blake A.J., Malook K., Wong H., Rehman S.-U-., Urease and α-chymotrypsin inhibitory activities of transition metal complexes of new Schiff base ligand: Kinetic and thermodynamic studies of the synthesized complexes using TG DTA pyrolysis, Thermochim. acta, 2013, 562C, 22-28.
- [16] Ikram M., Rehman S.-U., Rehman S., Baker R.J., Schulzke C., Synthesis, characterization and distinct butyrylcholinesterase activities of transition metal [Co(II), Ni(II), Cu(II) and Zn(II)] complexes of 2-[(E)-(quinolin-3-ylimino)methyl]phenol, Inorg. Chim. Acta, 2012, 390, 210-216.
- [17] Rehman S.-U-., Ikram M., Rehman S., Jan N., Synthesis and characterization of Ni(II), Cu(II) and Zn(II) nitrate coordination complexes of modified hydrazine, Journal of Mexican Chemical Society, 2011, 55(3), 164-167.
- [18] Rehman S.-U-., Ikram M., Rehman S., Akhtar G., Ullah F., Synthesis, Physicochemical and Biological Studies of Complexes of 2-Aminobenzohydrazine with Co(II), Ni(II), Cu(II) and Zn(II) Chlorides, Synthesis and Reactivity in Inorganic Metal Organic and Nano metal Chemistry, 2010, 40(10), 847-854.
- [19] Dolomanov O.V., Bourhis L.J., Gildea R.J., Howard J.A.K., Puschmann H., OLEX2:a complete structure solution, refinement and analysis program, J. Appl. Cryst. 2009; 42:
- [20] Sheldrick GM. A short history of SHELX, Acta Crystallogr. A, 2008, 64, 112-122.
- [21] Khan I., Ali S., Hameed S., Rama N.H., Hussain M.T., Wadood A., Synthesis, antioxidant activities and urease inhibition of some new 1,2,4-triazole and 1,3,4-thiadiazole derivatives, Eur. J. Med. Chem., 2010, 45, 5200-5207.
- [22] Cannell R.J.P., Kellam S.J., Owsianka A.M., Walker J.M., Results of a large scale screen of microalgae for the production of Protease inhibitors, Planta Med., 1988, 54, 10-14
- [23] Horowitz H.H., Metzger G., A new analysis of thermogravimetric traces, Anal. Chem. 1963, 35(10), 1464-
- [24] Olszak-Humienik M., Mozejko J., Thermodynamic functions of activated complexes created in thermal decomposition processes of sulphates, Thermochim. Acta, 2000, 344, 73-79.
- [25] Ünver H., Hayvalı Z., Synthesis, spectroscopic studies and structures of square-planar nickel(II) and copper(II) complexes derived from 2-{(Z)-[furan-2-ylmethyl]imino]methyl}-6methoxyphenol, Spectrochim. Acta Part A, 2010, 75, 782-788.
- [26] Pal S.N., Pal S., A Diruthenum(III) Complex Possessing a Diazine and Two Chloride Bridges: Synthesis, Structure, and Properties, Inorg. Chem., 2001, 40, 4807-4810.

- [27] Musiani F., Arnofi E., Casadio R., Ciurli S., Structure based computational study of catalytic and inhibition mechanisms of urease, J. Biol. Inorg. Chem., 2001, 6(3), 300-314.
- [28] Özer C.K., Arslan H., Derveer D.V., Külcü N., Synthesis and Characterization of N-(Arylcarbamothioyl)cyclohexanecarboxamide Derivatives: The Crystal Structure of N-(Naphthalen-1-ylcarbamothioyl)cyclohexanecarboxamide, Molecules., 2009, 14, 655-666.
- [29] Tinguiano D., Sy A., Thiam I.E., Gaye M., Retailleau P., (S,E)-3-[(2-Hy-droxy-benzyl-idene)amino]-2-(2-hy-droxy-phen-yl)-2,3dihydro-quinazolin-4(1H)-one, Acta Crystallogr., Sect.E:Struct. Rep.Online, 2012, 68, o2374-2375.